Phase stability and superconductivity of lead hydrides at high pressure

Bole Chen,[1,2,3] Lewis J. Conway,[3] Weiguo Sun,[2,3] Xiaoyu Kuang,[2] Cheng Lu,[1,*] and Andreas Hermann[3,†]

[1]*School of Mathematics and Physics, China University of Geosciences (Wuhan), Wuhan 430074, China*

[2]*Institute of Atomic and Molecular Physics, Sichuan University, Chengdu 610065, China*

[3]*Centre for Science at Extreme Conditions and SUPA, School of Physics and Astronomy, The University of Edinburgh, Edinburgh EH9 3FD, United Kingdom*

(Received 28 September 2020; revised 1 December 2020; accepted 5 January 2021; published 19 January 2021)

Density functional theory calculations and crystal structure predictions using the particle swarm optimization method have been combined to determine stable hydrides of lead under pressure. In contrast to other group-IVa hydrides, the stoichiometry PbH_6 is the first hydride to become stable, at just under 1 Mbar. For two previously studied stoichiometries, PbH_4 and PbH_8, energetically more favorable phases were identified to become stable around 2 Mbar. In all structures, the hydrogenic sublattices comprise negatively charged $H_2^{\delta-}$ molecules. Competitive PbH_4 and PbH_6 structures are layered. PbH_6 features H_2 molecules intercalated between hcp Pb layers, the stable phase of dense pure lead, thus offering a potentially straightforward route towards synthesis. In PbH_8, the Pb lattice adapts a β-Sn structure, and hydrogen atoms form quasi-one-dimensional-chains. All structures were found to be metallic and to feature superconductivity in their respective stability range, with moderately high T_c in the range 60–100 K for PbH_4 and PbH_6 and 161–178 K for PbH_8.

DOI: 10.1103/PhysRevB.103.035131

I. INTRODUCTION

Compressed metallic hydrogen was proposed as a potential high-temperature superconductor based on BCS theory [1], inspiring numerous searches for metallic hydrogen. Recently, conductivity measurements showed that hydrogen conducts above 360 GPa [2]; IR absorption measurements showed an abrupt drop in transmission at 420 GPa [3], while optical measurements found a shiny phase at 495 GPa [4]. However, these pressures are very hard to reach, and detailed measurements are difficult. As a means of inducing metallicity in hydrogen in less extreme conditions, chemical precompression was suggested as a feasible pathway to produce metallic and superconducting hydrogen-rich compounds at lower pressure [5]. Along this line, a large number of stable hydride compounds with high transition temperature T_c were successfully predicted at low pressure using crystal structural searches and electronic structure calculations, such as SH_3 [6], CaH_6 [7], YH_{10} [8], and LaH_{10} [8]. Subsequent experimental results [9,10] demonstrated the ability of utilizing structural prediction and critical temperature calculations to discover potential hydrogen-rich compounds with high-T_c superconductivity. This stimulated further work on phase diagrams and potential superconductivity of hydrogen-rich compounds under high pressure, to the extent that a neural network was trained on data of predicted T_c to find regions in the periodic table that hold the most promise for superconducting hydrides [11]. The latter, of course, depends on accurate screening of potential hydride compounds and their electronic properties.

The group-IVa hydrides $(Si,Ge,Sn)H_4$ were at the forefront of studies of "chemically precompressed" hydrogen. They have been extensively investigated in the past 15 years and exhibit metallization at lower pressure than pure hydrogen. So far, the metallization of methane has not been successfully achieved in experiments, as it is likely to decompose before metallization would happen [12,13]. Eremets *et al.* [14] reported the transition of silane, SiH_4, from an insulating molecule to metal at 50 GPa and subsequent superconductivity with T_c of 17 K at 96 and 120 GPa using Raman scattering and electrical resistance measurements, though the reported metallization and superconductivity of silane could not be reconciled with later theoretical [15–17] and experimental [18–20] works. As the atomic radius increases, GeH_4 [21,22] and SnH_4 [23,24] have been predicted to possess higher T_c of 70–84 K at 500 GPa and 80 K at 120 GPa, respectively. As for PbH_4, Zaleski-Ejgierd *et al.* [25] reported several layered structures above 132 GPa which are different from other group-IVa hydrides, and all exhibit metallic behavior, but they did not investigate potential superconductivity.

For several group-IVa hydrides the predicted T_c values significantly increased after intercalating with additional H_2 [26,27]. In early experimental works [28–30], $SiH_4(H_2)_2$ and $GeH_4(H_2)_2$ were both observed with SiH_4 and GeH_4 molecules on fcc sites. The measured Raman and IR spectra for $SiH_4(H_2)_2$ [28] and $GeH_4(H_2)_2$ [30] revealed strong intermolecular interactions between SiH_4 (GeH_4) and H_2 at low pressure, which are demonstrated as the main reason for the predicted high-T_c superconductivity in *Ccca* $SiH_4(H_2)_2$ [26], while Zhong *et al.* mainly attributed the superconductivity in $P2_1/c$ $GeH_4(H_2)_2$ [27] to the vibrations of H_2 units. In the Pb-H system, Cheng *et al.* [31] combined extensive structural searches and electron-phonon coupling (EPC) calculations

*lucheng@calypso.cn

†a.hermann@ed.ac.uk

for $PbH_4(H_2)_2$ and proposed three thermodynamically stable phases, where the $C2/m$ phase has T_c of 107 K at 230 GPa. However, in contrast to all lighter group-IVa elements, lead does not form stable XH_4 molecules, and its hydrides seem to contain only H_2 molecules. There is therefore no reason to assume that PbH_4 or PbH_8, the stoichiometries favorable for the lighter group-IVa hydrides, are also the most relevant for lead, and a complete study of lead hydrides should include a wider range of compositions.

Here, we conduct a systematic computational study on the combination of the heaviest group-IVa element, Pb, with H atoms, aiming to systematically reveal the stable phases, their crystallographic structures, and electronic properties and examine potential superconducting properties. We find that a hydride compound so far not present in the group-IVa hydrides, PbH_6, is, in fact, the first lead hydride to form under pressure, while we also uncover more stable structures for PbH_4 and PbH_8 that feature at higher pressures. All structures are metallic and exhibit moderately high T_c in the range 61–178 K in their respective stability ranges.

II. COMPUTATIONAL METHODS

The CALYPSO code [32,33] based on the particle swarm optimization method has been successfully applied to a variety of binary [7,8,34] and ternary [34–36] hydrides at high pressure. Herein, variable-cell crystalline structure predictions for PbH_4, PbH_6, and PbH_8 containing 1 to 4 f.u./cell at 150 and 300 GPa were performed using the CALYPSO code. Generally, each search covered 50 generations and generated about 1500 trial structures. Structural relaxations, enthalpy, and electronic structure calculations were conducted using the Vienna Ab initio Simulation Package (VASP) [37] with the Perdew-Burke-Ernzerhof exchange-correlation functional [38] and projector augmented-wave data sets [39] that employed the $5d^{10}6s^26p^2$ and $1s^1$ valence electrons for Pb and H, respectively. An energy cutoff of 800 eV and k-grid density of $50/\text{Å}^{-1}$ for Brillouin zone samplings were used in enthalpy calculations and geometries optimized below a force convergence threshold of 1 meV/Å. Dynamical stability of the predicted structures was checked using the supercell approach as implemented in the PHONOPY code [40]. Bader charge analyses were performed with the CRITIC2 program [41,42]. Elastic constants were calculated to check the mechanical stability of predicted phases. Phonon dispersions, EPC, and superconductivities of the predicted stable phases were calculated within linear-response theory as implemented in the QUANTUM ESPRESSO package [43]. Ultrasoft pseudopotentials for Pb and H were adopted with a kinetic energy cutoff of 80 Ry. In EPC calculations, q meshes (k meshes) of $4 \times 4 \times 6$ ($24 \times 24 \times 36$) for $P6mm$ PbH_4, $8 \times 4 \times 8$ ($32 \times 16 \times 32$) for $Pmmn$ PbH_4, $8 \times 8 \times 3$ ($32 \times 32 \times 12$) for $C222_1$ PbH_6, and $4 \times 4 \times 4$ ($16 \times 16 \times 16$) for $Fddd$ PbH_8 were used.

III. RESULTS AND DISCUSSION

We performed enthalpy calculations for the different Pb-H compounds across the full pressure range 0–400 GPa. Full enthalpy curves including possible decomposition reactions for PbH_4, PbH_6, and PbH_8 as a function of pressure are shown in Fig. 1. The stable structures of Pb, H_2, PbH, and PbH_2 were taken from previously reported work [31,44,45]; in addition to the structures predicted in this work, previously reported stable structures of PbH_4 (space groups $Imma$, $P2_1/m$, and $Ibam$, labeled VII, IIa, and VIII in [25]) and PbH_8 ($C2/m$, $P\bar{1}$, and $Pnnm$ in [31]) were also taken into consideration. We also constructed the convex hulls [see Fig. 2(a)] by using formation enthalpies for the most favorable structure of each compound relative to elemental Pb and H_2 to determine energic stability. Combining the enthalpy curves and convex

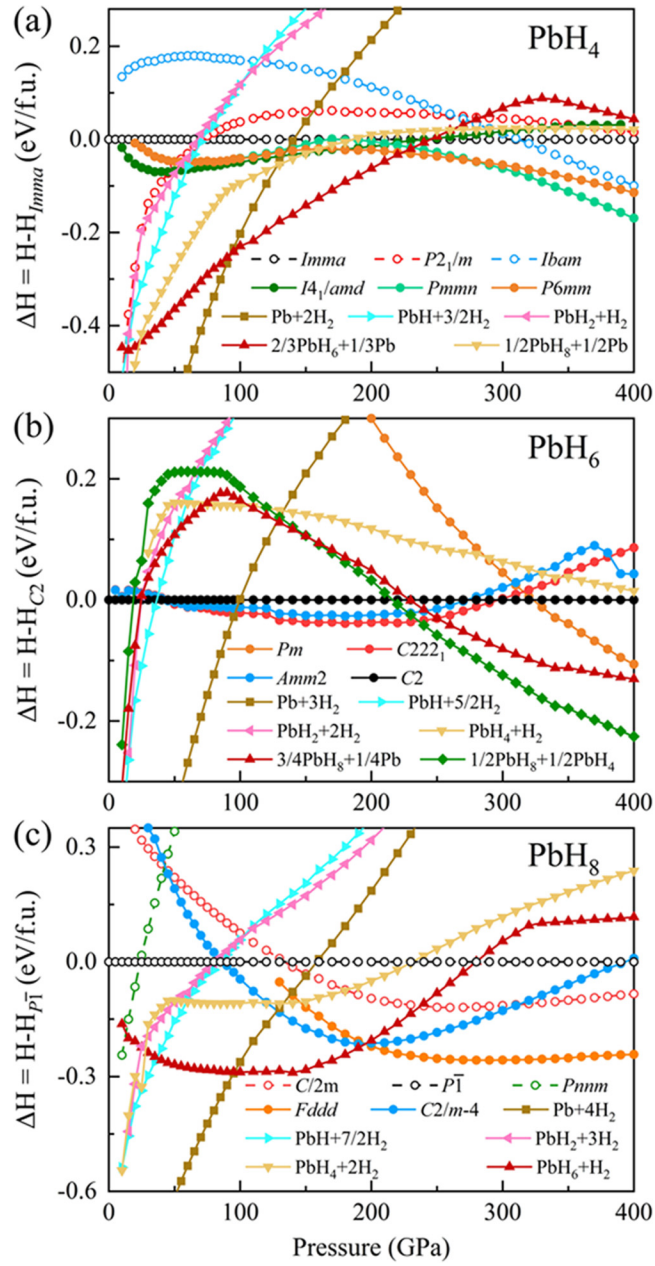

FIG. 1. The enthalpies per formula unit and decomposition enthalpies as a function of pressure for (a) PbH_4, (b) PbH_6, and (c) PbH_8. The reported structures for Pb [44], H_2 [45], and Pb-H [25,31] compounds are considered. Phases from the literature are drawn with open symbols and dashed lines; phases from this work are shown by solid symbols and solid lines.

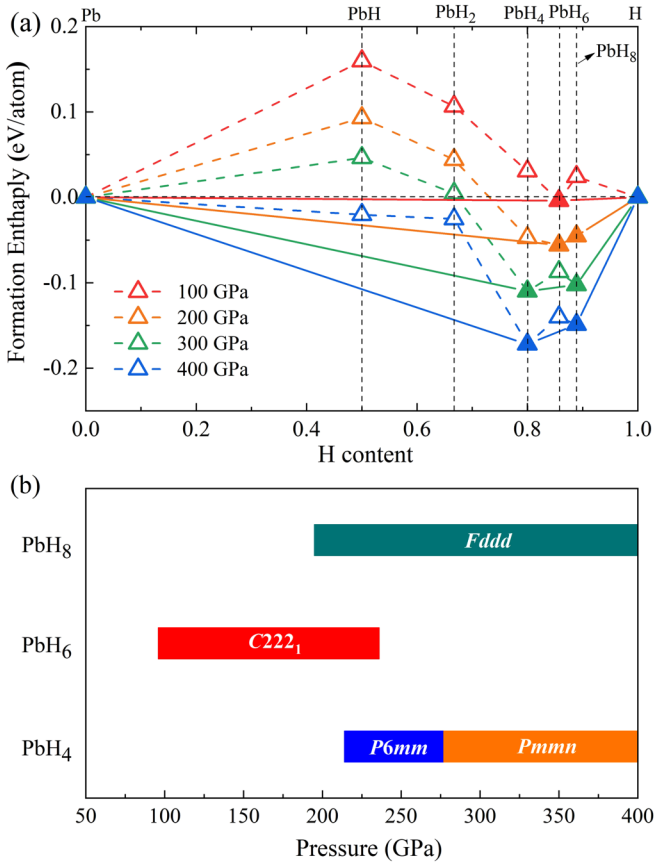

FIG. 2. Phase stabilities of lead hydrides. (a) Formation enthalpies of different Pb-H compounds at specific pressures. (b) Predicted ground state pressure-composition phase diagram of lead hydrides.

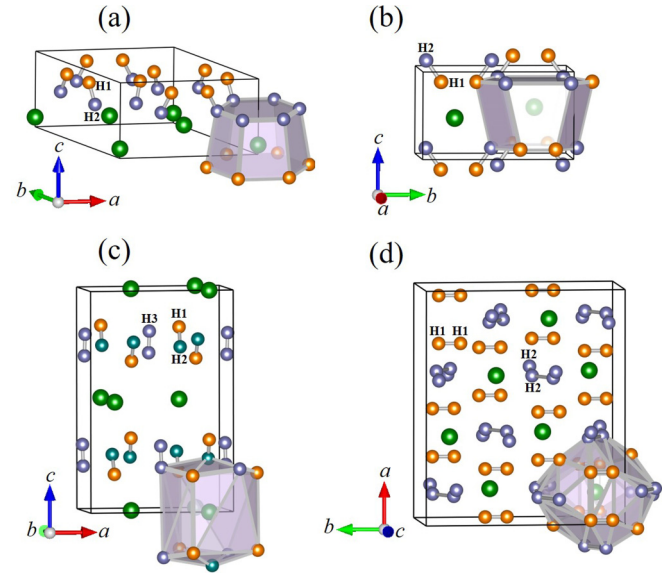

FIG. 3. Crystal structures of high-pressure lead hydrides. (a) *P6mm* PbH_4 at 250 GPa, (b) *Pmmn* PbH_4 at 300 GPa, (c) $C222_1$ PbH_6 at 100 GPa, and (d) $Fddd$ PbH_8 at 200 GPa. Green spheres represent Pb atoms, and yellow, light purple, and dark cyan represent crystallographically distinct H atoms as labeled. Coordination polyhedra of Pb atoms are indicated in each structure.

hull, the ground state phase diagram can be constructed and is depicted in Fig. 2(b). This differs substantially from the literature. First, PbH_6 emerges as the first lead hydride to become stable, at 96 GPa, and remains so, in a $C222_1$ structure, up to 236 GPa. Previously suggested structures for PbH_4 are superseded by the presently predicted *P6mm* and *Pmmn* phases [see Fig. 1(a)]; the onset of stability for *P6mm* PbH_4, due to the presence of PbH_6, is delayed to 214 GPa. At 277 GPa the *Pmmn* phase becomes more stable than *P6mm*. For PbH_8 [see Fig. 1(c)], a predicted $Fddd$ phase is more energetically favored than the $C2/m$ phase (reported previously stable above 160 GPa [31]) and becomes stable above 195 GPa.

Zero-point (ZP) vibrational energy can play a crucial role in changing relative stabilities because of the pronounced nuclear quantum effects in hydrogen-rich compounds. To gauge their importance here, we recalculated the formation enthalpies of various Pb-H compounds, Pb, and H_2 at 50, 100, 150, 200, and 300 GPa, including ZP vibrational energy at the harmonic level, then reconstructed the convex hulls as displayed in Fig. S1 in the Supplemental Material (SM) [46]. The phase diagram of stable phases remains qualitatively unchanged (see Fig. S2): PbH_6 becomes the first stable hydride, at a slightly lower pressure of 91 GPa, followed by PbH_8 and PbH_4 around 150 GPa; the latter two remain stable up to at least 300 GPa. A monoclinic $C2/m$-4 phase of PbH_8 emerges as stable in a small pressure range. To further examine the dynamical stability of the predicted phases, we show the phonon dispersions of the different hydrides across their respective stability ranges in Fig. S3; the absence of any imaginary modes confirms their dynamical stability. The $C222_1$ PbH_6 phase remains dynamically stable down to at least 50 GPa. The calculated elastic moduli are summarized in Table S2, confirming that the predicted Pb-H phases are also mechanically stable since they all meet the mechanical stability criteria [47].

The predicted stable structures of PbH_4, PbH_6, and PbH_8 at specific pressures are displayed in Fig. 3 and described below in more detail; their crystal structures are listed in Table S1. In general, all stable compounds comprise isolated Pb atoms in matrices of H_2 molecules; this is qualitatively similar to what has been found previously [25,31]. The two new structures for PbH_4, *P6mm* and *Pmmn*, are shown in Figs. 3(a) and 3(b). In both structures, Pb atoms are 12-fold coordinated to surrounding H_2 molecules and at the centers of distorted hexagonal prisms. In *P6mm* PbH_4 at 250 GPa the nearest Pb-H separations are 1.958–1.987 Å [Fig. 3(a)], and in *Pmmn* PbH_4 at 300 GPa they are 1.871–1.998 Å [Fig. 3(b)]. The Pb atoms form slightly distorted simple hexagonal lattices, with H_2 molecules placed in their trigonal prismatic holes; thus, both structures, in the form $Pb(H_2)_2$, approximate the $CaHg_2$ (or AlB_2) structure type. The H_2 molecules in both structures have significantly elongated bond lengths: 0.809 Å in *P6mm* PbH_4 and 0.831 Å in *Pmmn* PbH_4.

The $C222_1$ PbH_6 and $Fddd$ PbH_8 phases retain many of the same structural motifs, but the higher hydrogen content changes the Pb coordination environment and gives more variability to the hydrogenic sublattices [see Figs. 3(c) and 3(d)]. The Pb lattice in $C222_1$ PbH_6 is hcp but (due to H_2

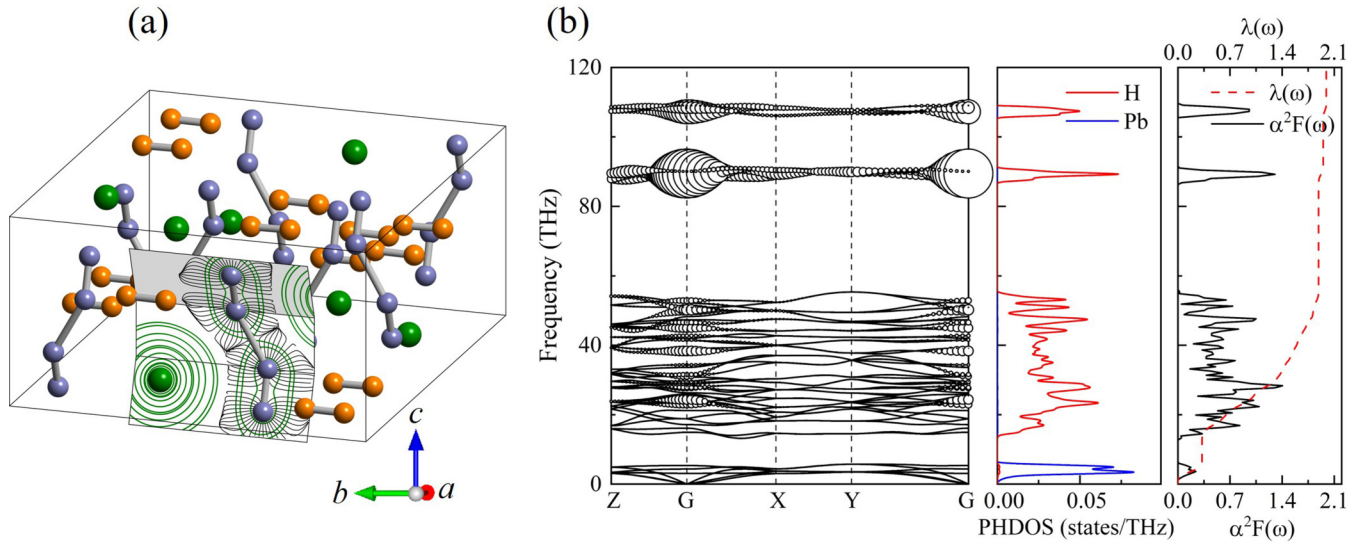

FIG. 4. (a) Charge density topology analysis of $Fddd$ PbH_8 with cross sections that show charge density contours (green lines) and gradients (black lines). (b) Calculated phonon dispersion (the radius of the black circle is proportional to the phonon linewidth), projected phonon density of states, Eliashberg phonon spectral function $\alpha^2F(\omega)$, and integrated electron-phonon coupling $\lambda(\omega)$ for $Fddd$ PbH_8 at 200 GPa.

intercalation) with an extremely large c/a ratio of 2.67. Note that the Pb lattice in PbH_6 is the same as the high-pressure elemental form of Pb. The formation of PbH_6 could therefore progress against relatively low reaction barriers, involving only the intercalation of H_2 molecules between the layers of high-pressure hcp Pb. The Pb lattice in $Fddd$ PbH_8 has the β-Sn structure. While in $C222_1$ PbH_6 the two types of H_2 molecules have very similar H-H distances of 0.769 Å (H1-H2) and 0.770 Å (H3-H3), the $Fddd$ PbH_8 structure features two very different types of H_2 molecules, with separations of 0.777 and 0.817 Å. The first type, H1-H1 (0.777 Å), is along the b axis [see Fig. 3(d)]. The second type, H2-H2 (0.817 Å), is roughly along the c axis and forms quasi-one-dimensional (quasi-1D) chains along that axis.

To understand the drivers of formation of these hydrides better, we analyzed their chemical bonding in both real space and reciprocal space. Real-space analyses are based on Bader's quantum theory of atoms in molecules [48], in which a topological analysis of the charge density identifies critical points, lines, and surfaces. Critical points are associated with ions or center points of bonds which appear as maxima or saddle points in the charge density. For ionic critical points, integrating the charge within the charge basin volume gives an effective charge. For bond critical points (BCPs), the value (ρ) and the curvature ($\nabla^2\rho$) of the charge density at the BCP help to characterize the bonding type and strength, with ionic bonds having positive curvature and lower charge densities at the BCP. These regions can be calculated and visualized using gradient path analyses with gradient paths seeded from the critical points, as seen in Figs. 4 and S4. We find that the extended H_2 bond lengths are due to partial negative charge acquired from the Pb atoms. From the Bader-Yu-Trinkle charge analysis listed in Table I, each H_2 unit in $P6mm$ PbH_4, $Pmmn$ PbH_4, $C222_1$ PbH_6, and $Fddd$ PbH_8 accepts approximately 0.330e, 0.354e, 0.154/0.150e and 0.148/0.274e from Pb atoms, respectively. These electrons partially occupy the antibonding orbital of the H_2 molecules, and the bond lengths in the H_2 units increase roughly linearly with the number of electrons transferred from Pb to H. The charge transfer from the Pb atom to each H_2 unit increases with pressure (in $C222_1$ PbH_6 at 200 GPa it is 0.158e) and, at comparable pressures, increases with hydrogen content. The topological structure of the charge density for the four structures is shown in Figs. 4 and S4, and properties of the resulting BCPs and charge basins are also listed in Table I. These data confirm a strong correlation between H_2 bond length increase and reduction in covalent bond strength (as measured through BCP charge density ρ_{BCP} and the Laplacian $\nabla^2\rho_{BCP}$).

For reciprocal-space analysis of the bonding in these hydrides, we show in Fig. 5 the electronic band structures and densities of states (DOSs), both projected onto atomic H s and Pb $s/p/d$ orbitals. First, the data indicate good metallic character, without noticeable pseudogaps, for all lead hydrides. The DOSs at the Fermi level mainly originate from the Pb atoms, with substantial contributions from H-derived states. Some bands that cross the Fermi levels show a signature of mixed character, and therefore hybridization of Pb and H states (for example, along Γ-A in $P6mm$ PbH_4 or along Γ-Z in $Pmmn$ PbH_4), but the majority of bands are dominated by clear Pb p or H s character. An alternative to quantify interatomic interactions is the crystal orbital Hamilton population (COHP) analysis [49,50]. In Fig. 6 we show the COHP projected onto individual atom pairs: averaging the first coordination shell Pb-H contacts, the intramolecular H-H covalent bonds, and intermolecular H $\cdots$ H contacts. In plotting the negative projected COHP (-PCOHP), positive (negative) values refer to bonding (antibonding) interactions. Table II gives the integrated COHP (ICOHP) up to the Fermi level, a measure of total atom pair interaction strength. First, we note that intramolecular H-H bonds all have antibonding character at the Fermi level, corroborating the partial charge analysis above; the H-H ICOHP also correlates with charge

TABLE I. H_2 molecular parameters: bond length, bond critical point charge density ρ_{BCP}, and the Laplacian $\nabla^2\rho_{BCP}$. Bader-Yu-Trinkle (Y-T) charge analysis for all atoms, electron-phonon coupling (EPC) parameters λ, electronic density of states at the fermi level $N(E_f)$, logarithmic average phonon frequency ω_{log}, and superconducting critical temperatures T_c of Pb-H structures, all at selected pressures. For PbH_6 and PbH_8, two sets of H_2 bond data refer to the H_3-H_3 and H_1-H_2 bonds, and the H_1-H_1 and H_2-H_2 bonds, respectively (see Fig. 3).

	Parameter	*P6mm* PbH_4 250 GPa	*Pmmn* PbH_4 300 GPa	$C222_1$ PbH_6 100 GPa		*Fddd* PbH_8 200 GPa	
H_2 bonds	Distance (Å)	0.809	0.831	0.770	0.769	0.777	0.817
	ρ_{BCP}	0.239	0.228	0.261	0.260	0.262	0.232
	$\nabla^2\rho_{BCP}$	−0.819	−0.570	−1.288	−1.193	−1.147	−0.749
Y-T charge	H AVG charge	1.165	1.177	1.077	1.075	1.074	1.137
integrals	Pb AVG charge	13.336	13.292	13.548		13.159	
EPC	$\omega_{log}(K)$	771.14	843.00	566.11		1000.93	
	λ	1.21	1.24	2.03		1.99	
	$N(E_f)$	9.59	6.53	9.29		9.94	
	T_c (K), μ^*=0.10	69.68	78.69	102.94		178.04	
	T_c (K), μ^*=0.13	61.88	70.15	93.33		161.59	

transfer: the larger the H partial charge is, the lower the covalent H-H bond strength is. Second, we note that Pb-H interactions are noticeable as measured by ICOHP but are dominated by interactions of H *s* with Pb *d* states about 20 eV below the Fermi energy. The Pb-H interactions around the Fermi level are very weak, and Pb-H hybridization should not be a major factor for properties that depend on the states near the Fermi energy (such as electron-phonon coupling; see the next paragraph). Third, intermolecular H · · · H interactions are weak but increase with pressure; the *Fddd* PbH_8 phase is an outlier with comparatively strong H2· · · H2 interactions.

Metallic hydrides were previously shown to be potential superconductors at high pressure. Thus, we conducted EPC calculations for the four metallic Pb-H compounds identified

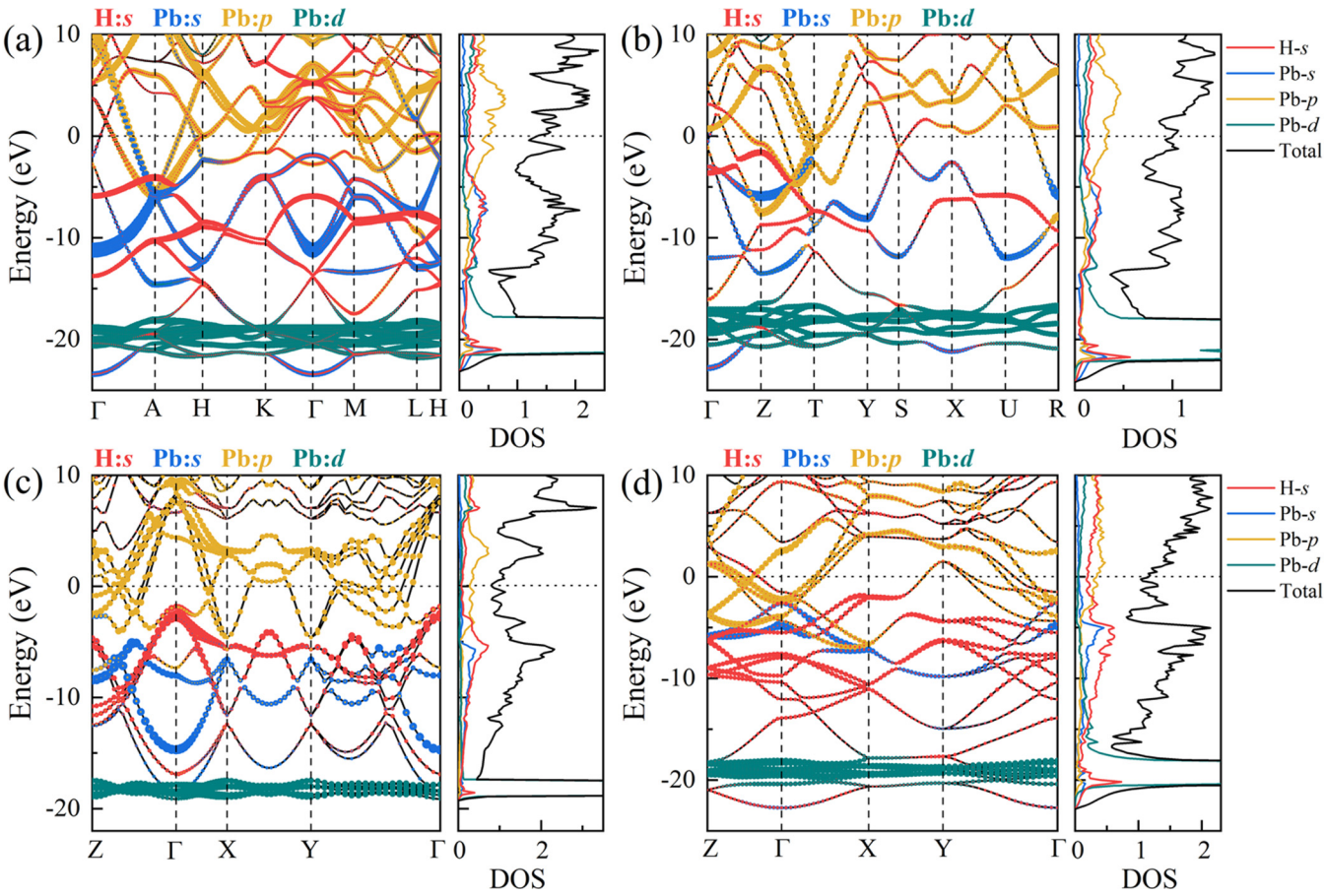

FIG. 5. The calculated electronic band structure and projected DOS for (a) *P6mm* PbH_4 at 250 GPa, (b) *Pmmn* PbH_4 at 300 GPa, (c) $C222_1$ PbH_6 at 100 GPa, and (d) *Fddd* PbH_8 at 200 GPa.

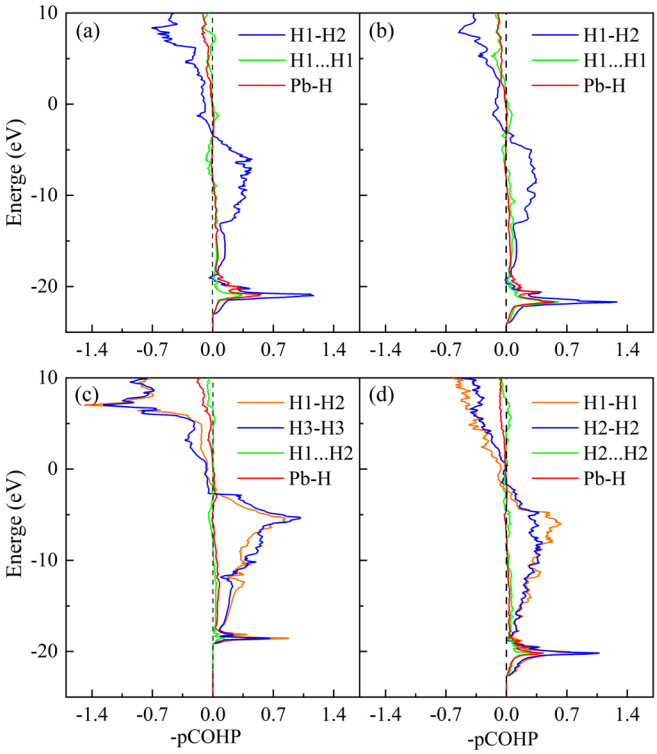

FIG. 6. -PCOHP for pairs of Pb-H, H-H, and H···H in (a) *P6mm* PbH_4 at 250 GPa, (b) *Pmmn* PbH_4 at 300 GPa, (c) $C222_1$ PbH_6 at 100 GPa, and (d) *Fddd* PbH_8 at 200 GPa. Energies are normalized to the respective Fermi level.

above. Relevant properties, including T_c at relevant pressures, are listed in Table I. T_c values were estimated from the modified McMillan-Allen-Dynes equation [51]: $T_c = \frac{\omega_{\log}}{1.2}\exp[-\frac{1.04(1+\lambda)}{\lambda-\mu^*(1+0.62\lambda)}]$, where the screened Coulomb potential parameter μ^* was set to 0.1–0.13, as previously suggested for metal hydrides [5]. For λ larger than 1.6, strong-coupling and shape correction multipliers (f_1 and f_2) are considered in the T_c equation: $T_c = f_1 f_2 \frac{\omega_{\log}}{1.2}\exp[-\frac{1.04(1+\lambda)}{\lambda-\mu^*(1+0.62\lambda)}]$. All four structures have moderately high T_c. The *Fddd* PbH_8 phase's $T_c = 161.59$ K and averaged EPC coupling $\lambda = 1.99$ are significantly higher than the previously reported $T_c = 107$ K and $\lambda = 1.296$ in $C2/m$ $PbH_4(H_2)_2$ [31], while superconductivity of PbH_4 or PbH_6 has not been reported previously. We find a gradual increase in T_c with increasing hydrogen content; the pressure dependence of T_c (see Table S3) is relatively weak.

TABLE II. Integrated COHP (ICOHP) up to the Fermi level for different atom pairs in Pb-H compounds: Pb-H, averaged over all first coordination shell Pb-H contacts; H-H, intramolecular covalent contacts; and H···H, closest intermolecular contacts.

Compound	ICOHP (eV/atom pair)		
	Pb-H	H-H	H···H
P6mm PbH_4 (250 GPa)	−1.03	H1-H2: −4.23	H1···H1: −0.52
Pmmn PbH_4 (300 GPa)	−1.02	H1-H2: −3.87	H1···H1: −1.22
$C222_1$ PbH_6 (100 GPa)	−0.88	H1-H2: −5.34, H3-H3: −5.65	H1···H2: −0.18
Fddd PbH_8 (200 GPa)	−0.69	H1-H1: −5.33, H2-H2: −4.66	H2···H2: −0.79

We analyze the *Fddd* PbH_8 phase in more detail, while the EPC results for the other three structures are shown in Fig. S4 and discussed in the SM. The electronic charge contour lines and gradient paths, the phonon dispersion curves overlaid with phonon linewidth $\gamma(\omega)$, phonon DOS, EPC parameter λ, and Eliashberg spectral function $\alpha^2F(\omega)$ of *Fddd* PbH_8 at 200 GPa are compiled in Fig. 4. The H_2 molecules in *Fddd* PbH_8 [see Figs. 4(a) and 6(d) and Tables I and II] are clearly distinct; the H1-H1 set is weakly negatively charged (partial charge $\delta_H = -0.074$) and strongly bound ($\nabla^2\rho_{BCP} = -1.147$, ICOHP $= -5.33$ eV). The H2-H2 set has larger partial charge ($\delta_H = -0.137$), weaker covalent bonding ($\nabla^2\rho_{BCP} = -0.749$, ICOHP $= -4.66$ eV), and comparatively stronger intermolecular interaction ($\nabla^2\rho_{CP} = 0.065$, ICOHP $= -0.79$ eV), resulting in quasi-1D chains along the c axis. These can be seen from the three planes plotted in Fig. 4(a) that link two symmetrically equivalent H2-H2 molecules. Coupling between H_2 molecules was reported qualitatively for PbH_8 structures [31], while the formation of $(H_2)_2$ tetramers was identified in PbH_4 [25].

In the phonon dispersion [see the left panel of Fig. 4(b)], the largest phonon linewidths are present in the H2-H2 vibron modes; however, EPC is mostly contributed by the midfrequency range 12–55 THz, where phonon branches are related to intermolecular vibrations of H_2 molecules (78.7% in λ). Even though absolute bond strength in the hydrogen sublattice is small [as measured via intermolecular ICOHP(H···H)], its linear response to perturbations in the electronic structure (as quantified in the EPC) is considerable. This agrees with the previous report on $C2/m$ $PbH_4(H_2)_2$ [31], where coupling between H_2 and H_2 was argued to be the primary cause of T_c, and is also found in the other three Pb-H structures (see the SM). This sets lead hydrides apart from the early experimental observations in $SiH_4(H_2)_2$ and $GeH_4(H_2)_2$ [28,30], where strong intermolecular interactions between the SiH_4 (GeH_4) and H_2 molecules at low pressure were found to be the main reason for their superconductivity.

Significant electron-phonon coupling related to the intermolecular vibrations of the H_2 sublattices results in promising superconductivity in all compounds. There is a clear separation in T_c achievable in PbH_4 and PbH_6 (around 60–100 K) vs PbH_8 (around twice as high). The former structures are essentially layered, at least structurally (the electronic DOSs in Fig. 5 do not show square onsets typical for two-dimensional systems but are also entwined with the Pb 5*d* manifold of states). While this does not systematically affect their metallicity [as measured by $N(E_f)$; see Table I], it leads to weakened EPC λ or $\omega_{\log}$, thus limiting T_c. The PbH_8 structure is more three-dimensional in character (as seen through the Pb sublattice) and features stronger intermolecular H_2-H_2 interactions (as seen through COHP, once pressure differences are accounted for).

Its predicted T_c value of 161–178 K at 200 GPa places lead hydrides among the most promising *p*-block metal hydrides, where other candidates involve BiH_5, SbH_4, AsH_8, and $AlH_3(H_2)$ (all predicted T_c =118–151 K at 150–450 GPa

[52–55]), as well as GaH_3, InH_3, SnH_4, and PoH_4 (all $T_c <$ 100 K [23,56–58]). Some of these compounds feature atomic hydrogen (SbH_4, GaH_3) or H_3 units (BiH_5, InH_3), while others, like the lead hydrides, contain metal cations and negatively charged sublattices of H_2 molecules. The chemical precompression of hydrogen in the latter type achieves the equivalent of a metallic *molecular* phase of pure hydrogen, clearly at much lower pressures than in pure hydrogen itself. However, it has been argued that superconducting T_c's in these types of structures are ultimately limited by relatively low electron-phonon coupling, as the electronic structure is not heavily influenced by the motion of the negatively charged H_2 molecule [59,60]. While $\lambda = 1.99$ as found here for PbH_8 is clearly a respectable value, other hydrides—most prominently the rare-earth hydrides with atomic hydrogen cages [61]—that resemble the equivalent of metallic *atomic* hydrogen phases, again at much lower pressures than in pure hydrogen, seem to be able to overcome that limitation.

IV. CONCLUSIONS

In summary, we have systematically investigated hydrogen-rich Pb-H compounds under pressure using crystal structure prediction and electronic structure calculations. We suggest that PbH_6 should be the first lead hydride to form under pressure, below 100 GPa. Its structure, with H_2 molecules intercalated in a hcp Pb lattice, should make it accessible in experimental synthesis, and it could be quenched back to lower pressures: we find the $C222_1$ PbH_6 phase is dynamically stable down to at least 50 GPa. For previously investigated compositions PbH_4 and PbH_8, we report more stable structures. In particular, $Fddd$ PbH_8 was identified as being more energetically stable than previously predicted $C2/m$ $PbH_4(H_2)_2$ and features quasi-1D H_2 chains along the c axis. In all stable phases, hydrogen appears in molecular form surrounding Pb cations, and charge transfer from Pb to H_2 results in elongated H_2 molecules and metallic character in all hydrides. Despite being more stable than in previous reports, the structures discussed here show more promise for high-T_c superconductivity, which we predict to surpass 160 K in PbH_8.

ACKNOWLEDGMENTS

This work was supported in part by the National Natural Science Foundation of China (Grants No. U1804121, No. 11304167, and No. 11874043). L.J.C. acknowledges studentship funding from EPSRC under Grant No. EP/L015110/1. Computing resources provided by the UK national high performance computing service, ARCHER, and the UK Materials and Molecular Modelling Hub, which is partially funded by EPSRC (Grant No. EP/P020194) and for which access was obtained via the UKCP consortium funded by EPSRC Grant No. EP/P022561/1, are gratefully acknowledged. B.C. also acknowledges support from the China Scholarship Council.

[1] N. W. Ashcroft, Phys. Rev. Lett. **21**, 1748 (1968).
[2] M. I. Eremets, A. P. Drozdov, P. P. Kong, and H. Wang, Nat. Phys. **15**, 1246 (2019).
[3] P. Loubeyre, F. Occelli, and P. Dumas, Nature (London) **577**, 631 (2020).
[4] R. P. Dias and I. F. Silvera, Science **355**, 715 (2017).
[5] N. W. Ashcroft, Phys. Rev. Lett. **92**, 187002 (2004).
[6] D. Duan, Y. Liu, F. Tian, D. Li, X. Huang, Z. Zhao, H. Yu, B. Liu, W. Tian, and T. Cui, Sci. Rep. **4**, 6968 (2014).
[7] H. Wang, J. S. Tse, K. Tanaka, T. Iitaka, and Y. Ma, Proc. Natl. Acad. Sci. USA **109**, 6463 (2012).
[8] H. Liu, I. I. Naumov, R. Hoffmann, N. W. Ashcroft, and R. J. Hemley, Proc. Natl. Acad. Sci. USA **114**, 6990 (2017).
[9] A. P. Drozdov, P. P. Kong, V. S. Minkov, S. P. Besedin, M. A. Kuzovnikov, S. Mozaffari, L. Balicas, F. F. Balakirev, D. E. Graf, V. B. Prakapenka, E. Greenberg, D. A. Knyazev, M. Tkacz, and M. I. Eremets, Nature (London) **569**, 528 (2019).
[10] M. Somayazulu, M. Ahart, A. K. Mishra, Z. M. Geballe, M. Baldini, Y. Meng, V. V. Struzhkin, and R. J. Hemley, Phys. Rev. Lett. **122**, 027001 (2019).
[11] D. V. Semenok, I. A. Kruglov, I. A. Savkin, A. G. Kvashnin, and A. R. Oganov, Curr. Opin. Solid State Mater. Sci. **24**, 100808 (2020).
[12] L. J. Conway and A. Hermann, Geosciences **9**, 227 (2019).
[13] G. Gao, A. R. Oganov, Y. Ma, H. Wang, P. Li, Y. Li, T. Iitaka, and G. Zou, J. Chem. Phys. **133**, 144508 (2010).
[14] M. I. Eremets, I. A. Trojan, S. A. Medvedev, J. S. Tse, and Y. Yao, Science **319**, 1506 (2008).
[15] D. Y. Kim, R. H. Scheicher, S. Lebègue, J. Prasongkit, B. Arnaud, M. Alouani, and R. Ahuja, Proc. Natl. Acad. Sci. USA **105**, 16454 (2008).
[16] X. J. Chen, J. L. Wang, V. V. Struzhkin, H. K. Mao, R. J. Hemley, and H. Q. Lin, Phys. Rev. Lett. **101**, 077002 (2008).
[17] M. Martinez-Canales, A. R. Oganov, Y. Ma, Y. Yan, A. O. Lyakhov, and A. Bergara, Phys. Rev. Lett. **102**, 087005 (2009).
[18] O. Degtyareva, J. E. Proctor, C. L. Guillaume, E. Gregoryanz, and M. Hanfland, Solid State Commun. **149**, 1583 (2009).
[19] T. A. Strobel, A. F. Goncharov, C. T. Seagle, Z. Liu, M. Somayazulu, V. V. Struzhkin, and R. J. Hemley, Phys. Rev. B **83**, 144102 (2011).
[20] C. Narayana, R. G. Greene, and A. L. Ruoff, J. Phys.: Conf. Ser. **121**, 042019 (2008).
[21] H. Zhang, X. Jin, Y. Lv, Q. Zhuang, Q. Lv, Y. Liu, K. Bao, D. Li, B. Liu, and T. Cui, Phys. Chem. Chem. Phys. **17**, 27630 (2015).
[22] G. Gao, A. R. Oganov, A. Bergara, M. Martinez-Canales, T. Cui, T. Iitaka, Y. Ma, and G. Zou, Phys. Rev. Lett. **101**, 107002 (2008).
[23] J. S. Tse, Y. Yao, and K. Tanaka, Phys. Rev. Lett. **98**, 117004 (2007).
[24] G. Gao, A. R. Oganov, P. Li, Z. Li, H. Wang, T. Cui, Y. Ma, A. Bergara, A. O. Lyakhov, T. Litaka, and G. Zou, Proc. Natl. Acad. Sci. USA **107**, 1317 (2010).
[25] P. Zaleski-Ejgierd, R. Hoffmann, and N. W. Ashcroft, Phys. Rev. Lett. **107**, 037002 (2011).
[26] Y. Li, G. Gao, Y. Xie, Y. Ma, T. Cui, and G. Zou, Proc. Natl. Acad. Sci. USA **107**, 15708 (2010).

[27] G. Zhong, C. Zhang, X. Chen, Y. Li, R. Zhang, and H. Lin, J. Phys. Chem. C **116**, 5225 (2012).
[28] T. A. Strobel, M. Somayazulu, and R. J. Hemley, Phys. Rev. Lett. **103**, 065701 (2009).
[29] W. L. Yim, J. S. Tse, and T. Iitaka, Phys. Rev. Lett. **105**, 215501 (2010).
[30] T. A. Strobel, X. J. Chen, M. Somayazulu, and R. J. Hemley, J. Chem. Phys. **133**, 164512 (2010).
[31] Y. Cheng, C. Zhang, T. Wang, G. Zhong, C. Yang, X. J. Chen, and H. Q. Lin, Sci. Rep. **5**, 16475 (2015).
[32] Y. Wang, J. Lv, L. Zhu, and Y. Ma, Comput. Phys. Commun. **183**, 2063 (2012).
[33] Y. Wang, J. Lv, L. Zhu, and Y. Ma, Phys. Rev. B **82**, 094116 (2010).
[34] X. Li, Y. Xie, Y. Sun, P. Huang, H. Liu, C. Chen, and Y. Ma, J. Phys. Chem. Lett. **11**, 935 (2020).
[35] X. Liang, S. Zhao, C. Shao, A. Bergara, H. Liu, L. Wang, R. Sun, Y. Zhang, Y. Gao, Z. Zhao, X.-F. Zhou, J. He, D. Yu, G. Gao, and Y. Tian, Phys. Rev. B **100**, 184502 (2019).
[36] X. Liang, A. Bergara, L. Wang, B. Wen, Z. Zhao, X. F. Zhou, J. He, G. Gao, and Y. Tian, Phys. Rev. B **99**, 100505(R) (2019).
[37] J. Hafner, Comput. Phys. Commun. **177**, 6 (2007).
[38] J. P. Perdew, K. Burke, and M. Ernzerhof, Phys. Rev. Lett. **77**, 3865 (1996).
[39] G. Kresse and D. Joubert, Phys. Rev. B **59**, 1758 (1999).
[40] A. Togo and I. Tanaka, Scr. Mater. **108**, 1 (2015).
[41] A. Otero-de-la-Roza, M. A. Blanco, A. M. Pendás, and V. Luaña, Comput. Phys. Commun. **180**, 157 (2009).
[42] A. Otero-de-la-Roza and V. Luaña, J. Chem. Theory Comput. **6**, 3761 (2010).
[43] P. Giannozzi *et al.*, J. Phys.: Condens. Matter **21**, 395502 (2009).
[44] A. Y. Liu, A. García, M. L. Cohen, B. K. Godwal, and R. Jeanloz, Phys. Rev. B **43**, 1795 (1991).
[45] C. J. Pickard and R. J. Needs, Nat. Phys. **3**, 473 (2007).
[46] See Supplemental Material at http://link.aps.org/supplemental/10.1103/PhysRevB.103.035131 for crystallographic information, elastic moduli, phonon dispersion relations, and zero-point energy effects.
[47] F. Mouhat and F. X. Coudert, Phys. Rev. B **90**, 224104 (2014).
[48] R. F. W. Bader, *Atoms in Molecules: A Quantum Theory*, International Series of Monographs on Chemistry (Clarendon, Oxford, 1994).
[49] R. Dronskowski and P. E. Blöchl, J. Phys. Chem., **97**, 8617 (1993).
[50] S. Maintz, V. L. Deringer, A. L. Tchougreeff, and R. Dronskowski, J. Comput. Chem. **34**, 2557 (2013).
[51] P. B. Allen and R. C. Dynes, Phys. Rev. B **12**, 905 (1975).
[52] Y. B. Ma, D. F. Duan, D. Li, Y. X. Liu, F. B. Tian, H. Y. Yu, C. H. Xu, Z. J. Shao, B. B. Liu, and T. Cui, arXiv:1511.05291.
[53] D. Duan, Y. Liu, Y. Ma, Z. Shao, B. Liu, and T. Cui, Natl. Sci. Rev. **4**, 121 (2017).
[54] Y. Fu, X. Du, L. Zhang, F. Peng, M. Zhang, C. J. Pickard, R. J. Needs, D. J. Singh, W. Zheng, and Y. Ma, Chem. Mater. **28**, 1746 (2016).
[55] P. Hou, X. Zhao, F. Tian, D. Li, D. Duan, Z. Zhao, B. Chu, B. Liu, and T. Cui, RSC Adv. **5**, 5096 (2015).
[56] G. Gao, H. Wang, A. Bergara, Y. Li, G. Liu, and Y. Ma, Phys. Rev. B **84**, 064118 (2011).
[57] Y. Liu, D. Duan, F. Tian, H. Liu, C. Wang, X. Huang, D. Li, Y. Ma, B. Liu, and T. Cui, Inorg. Chem. **54**, 9924 (2015).
[58] Y. Liu, D. Duan, F. Tian, C. Wang, G. Wu, Y. Ma, H. Yu, D. Li, B. Liu, and T. Cui, RSC Adv. **5**, 103445 (2015).
[59] L. Zhang, Y. Wang, J. Lv, and Y. Ma, Nat. Rev. Mater. **2**, 17005 (2017).
[60] E. Zurek and T. Bi, J. Chem. Phys. **150**, 050901 (2019).
[61] F. Peng, Y. Sun, C. J. Pickard, R. J. Needs, Q. Wu, and Y. Ma, Phys. Rev. Lett. **119**, 107001 (2017).